Phase-ordering dynamics of the O(n) model: Exact predictions and numerical results

R. E. Blundell and A. J. Bray
Department of Theoretical Physics, The University, Manchester M13 9PL, England
(Received 17 September 1993)

We consider the pair correlation functions of both the order parameter field and its square for phase ordering in the O(n) model with a nonconserved order parameter in spatial dimension $2 \leq d \leq 3$ and spin dimension $1 \leq n \leq d$. We calculate, in the scaling limit, the exact short-distance singularities of these correlation functions and compare these predictions to numerical simulations. Our results suggest that the scaling hypothesis does not hold for the $d=2$ O(2) model.

PACS number(s): 64.60.Cn, 64.60.My

I. INTRODUCTION

When systems described by an order parameter with a continuous symmetry are quenched from a disordered phase into a broken symmetry phase, the phase ordering dynamics exhibited differs from that of systems with a discrete order parameter in a number of important ways. Many different systems in nature possess such symmetries, such as liquid crystals, superfluids, etc., and consequently there has been considerable interest recently in adapting methods originally developed to investigate discrete systems to encompass these new symmetries.

A major goal in the study of systems with both discrete and continuous symmetries, which has been partially fulfilled in recent years, is the approximate determination of the scaling function $f(x)$ for the two-point correlation function. Although exact calculations have proved possible only for physically uninteresting values of d and n [1], the spatial and spin dimensionalities, approximate theories [2–7] have been proposed which appear to agree closely with simulation results, both for the two-point correlation function of the order parameter field ϕ,

$$C_2(r,t)=\langle \phi(x,t)\phi(x+r,t)\rangle = f(r/L(t)) , \tag{1}$$

and its Fourier transform, the structure factor

$$S_2(k,t)=[L(t)]^d g(kL(t)) , \tag{2}$$

where $L(t)$ is the characteristic length scale at time t after the quench, the angular brackets represent an average taken over initial conditions, and the expected scaling forms have been anticipated in (1) and (2). In addition, the two-point function of the square of the field,

$$C_4^U(r,t)=\langle \phi^2(x,t)\phi^2(x+r,t)\rangle - \langle \phi^2(x,t)\rangle\langle \phi^2(x+r,t)\rangle , \tag{3}$$

(where U denotes "unnormalized") has recently been calculated within the framework of these approximate theories [8]. For scalar systems, the domain walls are sharp so this correlation function is equivalent to the defect-defect correlation function $\langle \rho(x,t)\rho(x+r,t)\rangle - \langle \rho\rangle^2$, where $\rho(x,t)$ is the defect density at x at time t. Another case of physical interest is that of a system with a complex scalar order parameter, e.g., superfluid helium, which can be regarded as an $n=2$ vector system. Here the correlation function of the order parameter $\phi(r,t)$ is not experimentally accessible. Physical probes couple to $\phi^2(r,t)$ instead, and so $C_4^U(r,t)$ is the relevant correlation function to consider.

It is generally accepted that, for systems with a nonconserved order parameter with $n \leq d$, topological defects play an important role in the process of phase ordering. For the O(n) model, one finds that the stable defects are interfaces for $n=1$, vortices for $n=2$, and monopoles for $n=3$ [9]. The idea we will use in the calculations presented in Sec. II is that the order parameter field close to one of these defects is determined solely by the geometric properties of the defect. Bray and Humayun have previously used this observation to calculate the singular short-distance behavior of the two-point correlation function, which is responsible for the power-law tail in the structure factor, and are therefore able to give an exact prediction of the *amplitude* of this tail [10] as well as confirming the result $S(k,t) \sim L^{-n} k^{-(d+n)}$ [2,3]. The latter generalizes the familiar "Porod's law" [11] to vector systems. We use similar ideas to calculate the short-distance form of $C_4(r,t)$, the correlation function of the square of the order parameter field, and in Sec. III D we compare simulation results to these predictions. We also discuss the validity of the dynamic scaling hypothesis in relation for the $d=2$ O(2) model, both in relation to our short-distance results and the simulation data.

II. EXACT RESULTS

In this section we present exact calculations of the short-distance behavior of the correlation functions discussed above. In principle, the idea behind the calculations can be applied to most correlation functions, although there seems little purpose in doing so as in general such correlation functions are not experimentally accessible.

The calculation of the singular behavior of the $C_2(r,t)$ function at short distance has, as we noted in the previous section, already been carried out by Bray and Humayun, so we will only summarize the calculation here and refer the reader to Ref. [10] for the details.

Consider the field ϕ at points x and $x+r$ in the presence of a point defect at the origin, appropriate to the situation $n=d$. Let us denote the defect density and average defect separation time t by $\rho(t)$ and $L(t)$, respectively, and the defect core size by a. Then for $a \ll |x| \ll L$ and $a \ll |x+r| \ll L$, the field ϕ at the two points will be saturated in length and can be taken to be directed radially outward from the origin [12]. We therefore have

$$\phi(x)\cdot\phi(x+r)=\frac{x\cdot(x+r)}{|x||x+r|} . \tag{4}$$

The singular short-distance behavior arises from the rapid spatial variation in the direction of the vector ϕ near the defect. Holding r fixed and averaging over all possible positions of the defect relative to the point x gives

$$C_{\rm sing}(r,t)=\rho(t)\int^{L} d^n x \left[\frac{x\cdot(x+r)}{|x||x+r|} - (\text{analytic terms}) \right] . \tag{5}$$

The integral in Eq. (5) is understood to be over all x which satisfy $|x|<L$. However, the subtraction of "analytic terms" from the integrand (i.e., analytic in r), sufficient to converge the integral at large $|x|$, enables us to evaluate the integral simply by extending it over all space.

After some algebra the expression for $C_{\rm sing}$ obtained is

$$\begin{aligned} C_{\rm sing}(r,t) &= nr^n\rho(t)\pi^{n/2-1}B\left(\frac{n+1}{2},\frac{n+1}{2}\right)\int_0^{\infty} du\, u^{-n/2-1}[e^{-u}-(\text{analytic terms})] \\ &= nr^n\rho(t)\pi^{n/2-1}B\left(\frac{n+1}{2},\frac{n+1}{2}\right)\Gamma(-n/2) . \end{aligned} \tag{6}$$

Again, the "analytic terms" above refer to sufficient terms in the expansion of $\exp(-u)$ in powers of u to converge the integral. In Eq. (6), $\Gamma(x)$ is the gamma function, and $B(x,y)$ the beta function.

For even n, the Γ function in Eq. (6) contains poles. To deal with these cases, we set $n=2m+\epsilon$ and expand the resulting expression, looking for the order unity term in ϵ. We will discuss this procedure more fully below in the context of the $C_4(r,t)$ function. Here we simply note that the principle effect is the introduction of an additional factor of $\ln r$.

To generalize this result to $n \le d$ is straightforward. In this situation, $\phi(r,t)$ lies in a plane normal to the defect, and so we resolve r into two parts; the component in this plane, $r_\perp$, and the component parallel to the defect core, $r_\parallel$. The average over the orientations of $r_\perp$ is simply the calculation for the point defects above, and so the required result comes from averaging Eq. (6) over the orientations of $r_\parallel$, with r replaced by its projection onto the plane, $r_\perp$. The final results for the singular short distance behavior of the two-point correlation function for general n and d in [10]

$$C_{\rm sing}(r,t)=\pi^{n/2-1}\frac{\Gamma(-n/2)\Gamma(d/2)\Gamma^2((n+1)/2)}{\Gamma((d+n)/2)\Gamma(n/2)} \times\rho(t)r^n . \tag{7}$$

Once again, for even n we expand the Γ function to extract the leading singular term, which leads to a factor of $\ln r$. Taking the Fourier transform of Eq. (7) gives the large k form of the structure factor, valid for general $n \le d$,

$$S(k,t)=\frac{\rho(t)}{\pi}(4\pi)^{(d+n)/2}\frac{\Gamma^2((n+1)/2)\Gamma(d/2)}{\Gamma(n/2)} \times k^{-(d+n)} , \tag{8}$$

valid for $ka \ll 1 \ll kL(t)$. We will compare this result to simulation data later. Before we do so, let us consider the short-distance behavior of the ϕ^2 correlation functions. Since ϕ^2 saturates to unity at late times, however, it is in practice more convenient to consider the pair correlation function of $1-\phi^2$. In particular, we are interested in this function normalized by its large-distance limit,

$$C_4(r,t)=\frac{\langle[1-\phi^2(x,t)][1-\phi^2(x+r,t)]\rangle}{\langle 1-\phi^2(x,t)\rangle\langle 1-\phi^2(x+r,t)\rangle} . \tag{9}$$

In soft spin models of Ising systems ($n=1$), the domain wall profile saturates exponentially fast to ± 1 and so the interfaces are sharp. This makes the calculation of $C_4(r,t)$ particularly simple. At any point in the system, $\langle[1-\phi^2(x,t)]\rangle$ is zero unless it is close to a domain wall, so we have immediately $\langle[1-\phi^2(x,t)]\rangle=a\rho(t)$, where this relation defines a as the domain wall width. For the product $[1-\phi^2(x,t)][1-\phi^2(x+r,t)]$ to be nonzero requires there to be an interface at x and at $x+r$. If r is small compared to the characteristic distance between interfaces, $L(t)$, then the two points must lie on the same interface. If we consider the point at x to lie on an interface, then the additional requirement that $x+r$ lies on the same interface gives a factor $aS_{d-1}/S_d r$, where S_d is the surface area of a d-dimensional unit sphere. We have, therefore, for $n=1$,

$$\langle[1-\phi^2(x,t)][1-\phi^2(x+r,t)]\rangle=a^2\frac{\rho(t)S_{d-1}}{S_d r} , \quad a \ll r \ll L(t) , \tag{10}$$

which gives, for $n=1$ and general d,

$$C_4(r,t)=\frac{\Gamma(d/2)}{\pi^{1/2}\Gamma((d-1)/2)}\frac{1}{\rho(t)r}, \quad a \ll r \ll L(t) . \tag{11}$$

The $d=3$ result was recently derived by Onuki [13].

For vector systems, the field far from a defect saturates as $1-\phi^2(x)=a^2/x^2$, where x is the distance from the defect, and a is the "size" of the defect core. It follows, therefore, that the short-distance behavior of $C_4(r,t)$ is given by

$$C_4(r,t)=\frac{\langle[1-\phi^2(x,t)][1-\phi^2(x+r,t)]\rangle}{\langle[1-\phi^2(x,t)]\rangle\langle[1-\phi^2(x+r,t)]\rangle}$$

$$=\left[\rho\int^L dx\frac{a^4}{x^2(x+r)^2}\right]\Big/\left[\rho\int^L dx\frac{a^2}{x^2}\right]^2, \quad (12)$$

provided the integrals are dominated by the field close to a defect. As before, we consider first the case of point defects, $n=d$, then generalize the result to $n\le d$. The denominator in Eq. (12) can be evaluated by changing to polar coordinates and gives, for $n=2$,

$$C_4^D=[2\pi a^2\rho\ln(L/a)]^2, \quad n=2 . \quad (13)$$

For $n>2$, the denominator in (12) is no longer dominated by the field close to the defects and so we cannot treat these cases in the same detail as for $n=2$. However, we can still evaluate the leading short-distance behavior of the numerator for $2<n\le 4$, and the leading short-distance singularity of the numerator for any $n\ge 2$.

To evaluate the numerator (denoted by superscript N), we first make a rescaling $x\to rx$, which gives

$$C_4^N(r,t)=\langle[1-\phi^2(x,t)][1-\phi^2(x+r,t)]\rangle$$

$$=\rho r^{n-4}\int_{a/r<x<L/r}dx\frac{a^4}{|x|^2|x+\hat{r}|^2} . \quad (14)$$

We now take $L/r\to\infty$ and $a/r\to 0$. For $n=2$, this makes the integrals become logarithmically divergent, and the following treatment applies strictly only for $2<n<4$, as we shall see below. We will discuss how the calculation is extended to $n=2$ later.

Using the integral representation $\int_0^\infty dv\exp(-uv)=1/u$ gives

$$C_4^N(r,t)=\rho a^4 r^{n-4}\int_0^\infty du\int_0^\infty dv\int_{-\infty}^\infty dx\exp(-u|x|^2-v|x+\hat{r}|^2) . \quad (15)$$

Evaluating the x integral first, followed by the (u,v) integrals, gives, after some algebra,

$$C_4^N(r,t)=\pi^{n/2}\frac{\Gamma((4-n)/2)\Gamma^2((n-2)/2)}{\Gamma(n-2)}\rho(t)a^4r^{n-4} . \quad (16)$$

To extend this result to $n<d$ we consider the vector r to be resolved into two components, $r_\perp$ and $r_\parallel$, where $r_\perp$ is the $(d-n)$-dimensional component of r in the plane perpendicular to the defect core and $r_\parallel$ is the orthogonal vector containing the remaining components of r. Using generalized spherical polar coordinates, the projection of r into the plane perpendicular to the defect is simply

$$|r_\perp|=r\prod_{i=1}^{d-n}|\sin\theta_i| . \quad (17)$$

To calculate $C_4^N(r,t)$ we use the result from Eq. (16) with r replaced by $r_\perp$ and average over all orientations of r, which is equivalent to averaging over the possible relative positions of the two points to the defect. This gives

$$C_4^N(r,t)=\pi^{n/2}\frac{\Gamma((4-n)/2)\Gamma^2((n-2)/2)}{\Gamma(n-2)}\rho(t)a^4\langle|r_\perp|^{n-4}\rangle . \quad (18)$$

To evaluate this expression we require the average

$$\langle|r_\perp|^{n-4}\rangle=r^{n-4}\left\langle\prod_{i=1}^{d-n}|\sin\theta_i|^{n-4}\right\rangle$$

$$=r^{n-4}\prod_{i=1}^{d-n}\left[\int_0^{\pi/2}d\theta_i(\sin\theta_i)^{n-4+d-1-i}\Big/\int_0^{\pi/2}d\theta_i(\sin\theta_i)^{d-1-i}\right]$$

$$=r^{n-4}\frac{\Gamma(n-2)\Gamma(d/2)}{\Gamma((n+d)/2-2)\Gamma(n/2)} . \quad (19)$$

Inserting this into (18) gives, for general $d\ge n$ and $2<n<4$, the short-distance behavior

$$C_4^N(r,t)=\pi^{n/2}\frac{\Gamma(2-n/2)\Gamma(d/2)\Gamma^2(n/2-1)}{\Gamma((n+d)/2-2)\Gamma(n/2)}\frac{\rho(t)a^4}{r^{4-n}} ,$$

$$a\ll r\ll L(t) . \quad (20)$$

In fact, this result gives the leading short-distance singularity in C_4^N for all $n>2$ (with the usual logarithmic factors for even n, which can be extracted by taking the limit from real n, appropriately). For $2<n\le 4$, it gives the leading short-distance behavior (not just the singularity), whereas, for $n>4$, C_4 saturates to a constant at short distance. [By "short distance" we mean, of course, $a\ll r\ll L(t)$ as usual]. Equation (20) implies the power-law tail $S_4(k,t)\sim\rho(t)k^{-(d+n-4)}$, for $d\ge n>2$, in the Fourier transform of C_4, a form first suggested in [8].

For $n=2$, there is a double pole in Eq. (20) for $d\neq 2$

and a single pole if $d=2$. These poles come from the lower end of the integration range in Eq. (14). In reality, $[1-\phi^2(x,t)]=a^2/x^2$ breaks down at $x\approx a$, so the integrals in Eq. (14) should be cut off at $r\simeq a$. The effect of introducing the cutoffs would be to eliminate the poles in Eq. (20). To extend this result to $n=2$, then, we set $n=2+\epsilon$ and expand the resulting expression to find the O(1) term in ϵ. The terms which are divergent as $\epsilon\to 0$ would be removed by a short-distance cutoff. This gives, for $d>2$,

$$C_4^N(r,t)=\rho(t)a^4\pi^{1+\epsilon/2}\frac{\Gamma(1-\epsilon/2)\Gamma(d/2)\Gamma^2(\epsilon/2)}{\Gamma((\epsilon+d)/2-1)\Gamma(1+\epsilon/2)r^{2-\epsilon}}$$
$$\to\frac{(d-2)\pi\rho(t)a^4\ln^2(r/a)}{r^2}\ , \tag{21}$$

on retaining the O(1) term in ϵ. We introduce factors of the form $\ln(r/a)$, rather than $\ln(r/L)$, say, because the cutoff required on the integrals is at $r=a$. For $d=2$, we need to take the limit $d\to 2$ before taking $n\to 2$. This leads to a cancellation of 2 of the Γ functions in Eq. (20), leaving

$$C_4^N(r,t)=\rho(t)a^4\pi^{1+\epsilon/2}\frac{\Gamma(1-\epsilon/2)\Gamma(\epsilon/2)}{\Gamma(1+\epsilon/2)r^{2-\epsilon}}$$
$$\to\frac{2\pi\rho(t)a^4\ln(r/a)}{r^2} \tag{22}$$

on retaining the O(1) term in ϵ. A direct calculation of the $n=2$ case with cutoffs on the integrals confirms these results, which are correct to leading logarithmic accuracy.

In the scaling limit, where r/L is kept fixed and $L\to\infty$, Eqs. (21) and (22) can be simplified using $\ln(r/a)=\ln(r/L)+\ln(L/a)\approx\ln(L/a)$. The normalized correlator $C_4=C_4^N/C_4^D$ is therefore, using (13) for C_4^D,

$$C_4(r,t)=\begin{cases}\dfrac{1}{2\pi\rho\ln(L/a)r^2}, & d=2 \quad (23)\\[2ex] \dfrac{d-2}{4\pi\rho r^2}, & d>2 \quad (24)\end{cases}$$

valid for $a\ll r\ll L(t)$. It is interesting that for $d>2$, the logarithms in C_4^N and C_4^D cancel to produce an expression in a conventional scaling form (with scaling variable ρr^2), as would be expected, whereas for $d=2$ a single logarithm remains in the denominator and therefore $C_4(r,t)$ does not have a scaling form at short distance [8]. This does not necessarily imply that there are no scaling phenomena in the $d=2$ O(2) model, but it does show that at least this correlation function does not scale. Taken together with evidence from the simulations of [14], and our own simulation results presented below, which indicate a multiplicity of length scales in this system as well as the calculation of Bray and Rutenberg of the energy dissipation [15], it now seems likely that scaling does not occur in the $d=2$ O(2) model.

In summary, we have exact predictions for the short-distance singularity of $C_2(r,t)$, or, equivalently, for the tail amplitude of the structure factor. We have also predicted the short-distance form of $C_4(r,t)$ for $n\le 2$, which for the two-dimensional (2D) XY model violates the scaling hypothesis. We now compare these results to computer simulations.

III. SIMULATION RESULTS

We now turn our attention to computer simulations of the O(n) model, the results of which we will compare to the above predictions. For $n>d+1$ there are no stable topological defects and for $n=d+1$ the defects are extended textures, the dynamics of which are not well understood. We therefore have restricted our investigations to $2\le d\le 3$ and $1\le n\le d$. The data from the $n=1$ simulations, some of which have already been published in another form [16], were provided by Sattler.

A. Cell dynamical simulations

The simulation of phase ordering using cell dynamical simulations (CDS) is by now standard [17]. The essential idea is to take a lattice of "soft" spins, corresponding to a coarse-grained order parameter field $\boldsymbol{\phi}(r,t)$, and update them with the mapping

$$\boldsymbol{\phi}_{n+1}(i)=D\left[\frac{1}{z}\sum_j\boldsymbol{\phi}_n(j)-\boldsymbol{\phi}_n(i)\right]$$
$$+E\hat{\boldsymbol{\phi}}_n(i)\tanh[|\boldsymbol{\phi}_n(i)|]\ , \tag{25}$$

where $\hat{\phi}=\boldsymbol{\phi}/|\boldsymbol{\phi}|$ [for scalar fields $\hat{\boldsymbol{\phi}}=\mathrm{sgn}(\phi)$], z is the number of nearest neighbors, and D and E are adjustable parameters, for which we chose the standard values $D=0.5$ and $E=1.3$ [14]. One can regard Eq. (25) as a discrete time-dependent Ginzburg-Landau (TDGL) equation in which the first term is the discretized Laplacian and the second is derived from a potential $V(\boldsymbol{\phi})$, the form of which has been chosen to keep the iteration process numerically stable and give the same attractors of the dynamics as the TDGL equation.

It is desirable when measuring C_2 to "harden" the spins, which is achieved by computing (for general n)

$$C_2^H(r,t)=\langle\hat{\phi}(x,t)\cdot\hat{\phi}(x+r,t)\rangle\ . \tag{26}$$

This reduces the effective size of the defects (domain walls, strings, etc.) to zero and hence scaling can be achieved at smaller values of r. Unfortunately, the same procedure cannot be applied to C_4 (which would vanish identically) and hence the scaling in this case for small r is considerably worse.

To measure the defect density in the vector systems we used two different algorithms. For the $d=n$ systems, the defects are points and so can be identified by looking for peaks in the local energy density $E_i=-\sum_{\langle j\rangle}\boldsymbol{\phi}_i\cdot\boldsymbol{\phi}_j$, where the sum is over the nearest neighbors of i. For the $d=3$ O(2) model, however, the defects are strings and

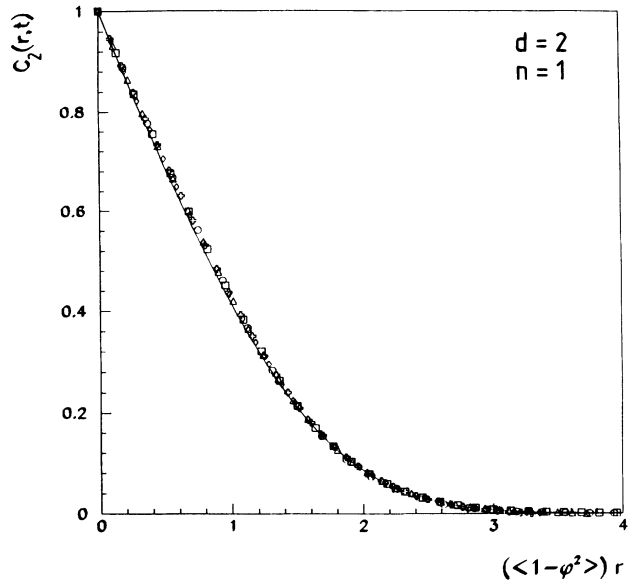

FIG. 1. The two-point correlation function of the $d=2$ scalar model. The data have been scaled using $\langle 1-\phi^2 \rangle$, which is proportional to the defect density (data courtesy of S. Sattler). The solid curve is the OJK prediction, with the horizontal axis scaled to give the best fit by eye to the data.

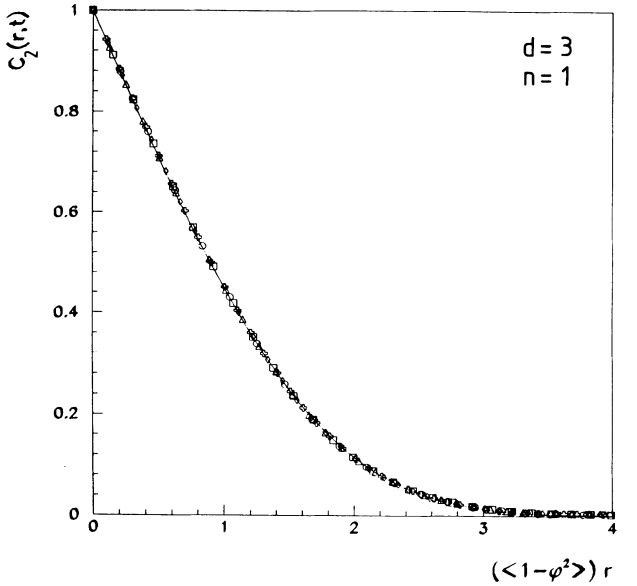

FIG. 3. Same as Fig. 1, but for the $d=3$ scalar model.

consequently this method is not so simple to use. Instead, we look for plaquettes around which the order parameter rotates through $\pm 2\pi$ radians and associate with each one a unit length of string. The same approach applies to the $d=2$ O(2) model gives results identical to those obtained with the algorithm based on the energy density. It is important to note, however, that the length of string given by this procedure is that given by a Manhattan metric, because the string is constrained to lie on the dual lattice. To compare to our calculations in Sec. II, which were based on a continuum description, requires that we use a Euclidean metric to measure the string length. Assuming that on a scale large compared to the lattice spacing the strings are isotropically oriented, we can convert between these two lengths by adjusting by a factor $[L_M/L_E]=\frac{3}{2}$ for $d=3$, where the brackets represent an average taken over all orientations of the string and L_M and L_E are the Manhattan and Euclidean

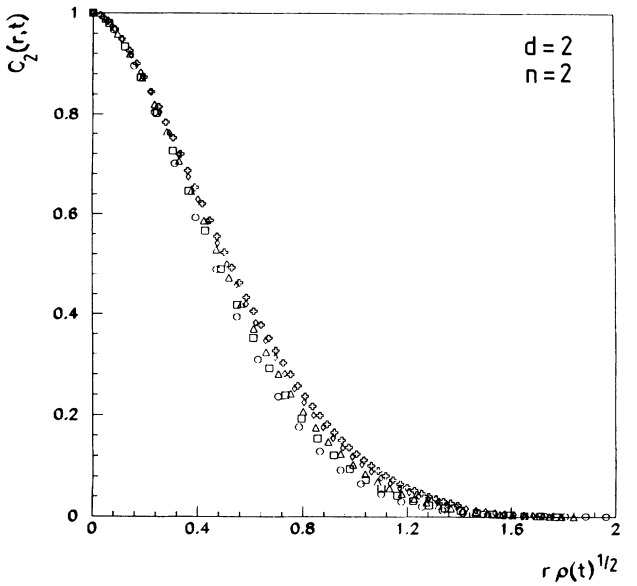

FIG. 2. The two-point correlation function of the $d=2$ O(2) model. The data have been scaled using the defect density.

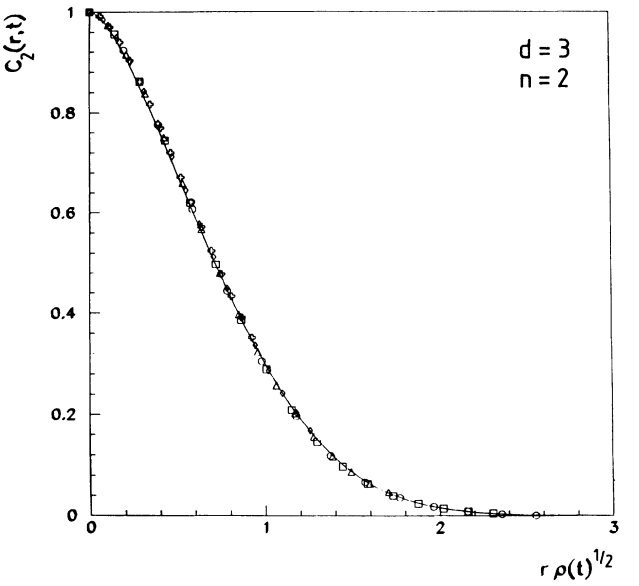

FIG. 4. The two-point correlation function of the $d=3$ O(2) model. The data have been scaled using the defect density. The solid curve is the BPT prediction, scaled to give the best fit by eye.

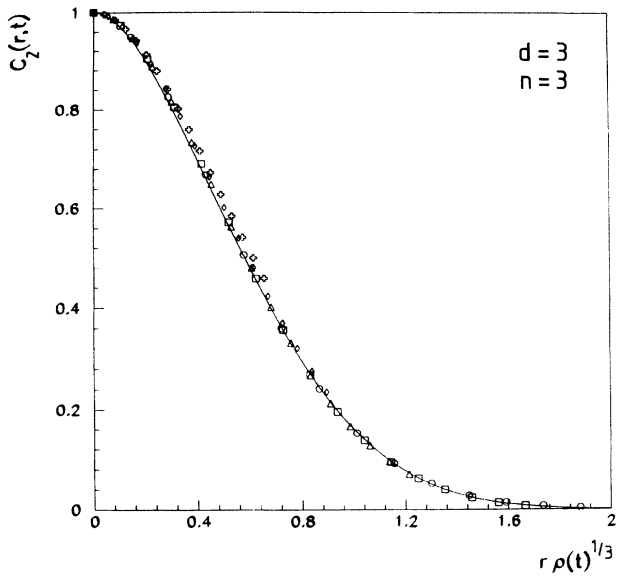

FIG. 5. Same as Fig. 4, but for the $d=3$ O(3) model.

lengths of the string.

The details of the simulations are shown in Table I. In all the following plots, we will use the symbols, circles, squares, triangles, diamonds, and crosses, to represent progressively later measurement times. The actual times to which these symbols refer can be read off from the table.

B. Dynamic scaling

We start the analysis of the data by considering a test of the dynamic scaling hypothesis. If this hypothesis is true, then the data for the two-point correlation function

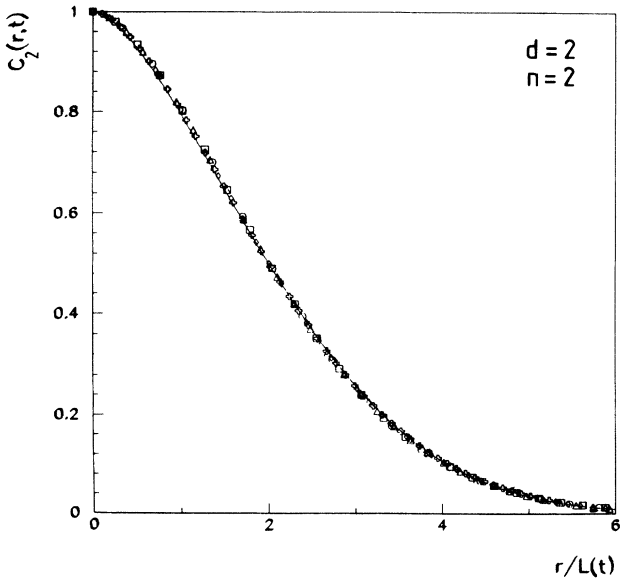

FIG. 6. The two-point correlation function for the $d=2$ O(2) model. The data have been scaled using the values $L(t)$, which gave the best scaling. The solid curve is the BPT prediction, scaled to give the best fit by eye.

TABLE I. Details of lattice size and number and length of runs for the numerical simulations.

Spatial dimension	2	2	3	3	3
Spin dimension	1	2	1	2	3
Lattice size	700	128	80	64	64
Realizations	30	500	45	250	150
Measurement times	400	80	100	40	40
	800	160	200	80	80
	1200	320	300	160	160
	1600	640	400	320	320
	2000	1280	500	640	640

$C_2(r,t)$ can be collapsed onto a single curve for each system by rescaling r by the characteristic scale $L(t)$. This scale can be defined in a number of ways. For example, it could be defined as the value of r for which $C_2(r,t)=\frac{1}{2}$, or even as the value which gives the best overall collapse of the data. A definition of this sort can be rather misleading, however, because a free parameter has been introduced for each value of t. As the form of $C_2(r,t)$ is rather featureless, it is not too surprising that a good collapse of the data can be obtained using methods such as these. An alternative and superior method is to use some characteristic length scale that is not directly related to $C_2(r,t)$. If the scaling hypothesis holds, then the defect density should scale as $\rho(t)\sim L^{-n}(t)$, and so it seems logical to use $r\rho^{1/n}(t)$ as the scaling variable. For the $n=1$ systems, we have used, instead of ρ, $\langle 1-\phi^2\rangle$, which scales in the same way as the true defect density. Figures 1 to 5 show the two-point correlation function scaled in this manner along with the theoretical predictions of Ohta, Jasnow, and Kawasaki (OJK) for the scalar systems and of Bray, Puri, and Toyoki (BPT) for the vector systems. The general form of these results is [2,3]

$$C_2(r,t)=\frac{n\gamma}{2\pi}\left[B\left(\frac{n+1}{2},\frac{1}{2}\right)\right]^2 F\left(\frac{1}{2},\frac{1}{2};\frac{n+2}{2};\gamma^2\right), \tag{27}$$

where $F(a,b;c;z)$ is the hypergeometric function, and $\gamma=\exp(-x^2/8)$, with $x=r/L(t)$ the scaling variable. In the theoretical curves, the horizontal scale has been adjusted to give the best fit.

Apart from $d=2$, $n=2$, the collapse of the data is excellent. For $d=3$, $n=3$ there is some evidence for finite size effects in the last data set, but otherwise the data scale well. We conclude that our numerical results are entirely consistent with the scaling hypothesis in these systems. It is clear, however, that for the $d=2$ O(2) model, i.e., the 2D XY model, the data do not scale. Furthermore, there is no evidence that the data at later times are approaching an asymptotic scaling curve. It is possible that the system has yet to reach the scaling regime even at the latest times, but considering how early the scaling regime is reached for the other systems, it is also possible that the scaling hypothesis fails for this system. It is interesting that the data can be collapsed to a single

curve by using values for $L(t)$ specially chosen to do so. The quality of the scaling achieved is as good as in any of the other systems (see Fig. 6). Bray and Rutenberg also find evidence that there may be scaling violations in the 2D XY model [15]. They conclude that energy dissipation due to the ordering process occurs significantly on all scales between the vortex core size and the intervortex spacing, suggesting there may not be a single length scale $L(t)$ that characterizes the system morphology. We recall that the exact short-distance behavior of $C_4(r,t)$ calculated in the previous section is also not in a scaling form.

In all cases, the theoretical curves fit the data very well. There are small discrepancies, but considering the approximations made in the calculation of these curves it is rather surprising how close they appear to be to the simulation data. We will see later, when we eliminate the free parameter required to compare the theory to simulation results, that there are in reality considerable discrepancies which are hidden by the introduction of the free parameter.

C. Growth laws

The growth law for the characteristic scale in systems with a nonconserved order parameter is expected to be $L(t)\sim t^{1/z}$, with $z=2$ [18,15]. By fitting a straight line to a log-log plot of the defect density against time we find the values of $1/z$ shown in Table II, which follow from the relation $L(t)\sim[\rho(t)]^{-n}$. After infinite time, all the defects should have been removed from the system. Consequently, we expect $\rho(t)$ plotted against $t^{-n/z}$ to be a straight line passing through the origin. Figure 7 shows these plots along with a straight line fit. To quote errors on the values of $1/z$ is somewhat misleading because the data at different times come from the same system and are therefore highly correlated. In all cases, however, a fit with $z=2$ is unacceptable, even for the $n=1$ systems. The reason for this is unclear. It could be that the systems have yet to reach their asymptotic behavior. A more likely explanation is the weak pinning effect on the defects, introduced by the lattice, which becomes more important at later times as the driving forces become weaker. However, the data are consistent with zero defect density for $t\to\infty$, so there is no direct evidence that defects become frozen at late times, as they do for hard-spin vector simulations [19]. It should be noted that previous simulations on vector systems also find growth exponents consistently less than $\frac{1}{2}$ [14,20].

For the 2D XY model, the growth laws for $[\rho(t)]^{-1/2}$ and $L(t)$, the length scale required to collapse the $C_2(r,t)$ function, are noticeably different. The log-log plots shown in Fig. 8 show clearly the different power laws involved. A least-squares fit gives $[\rho(t)]^{-1/2}\sim t^{0.37}$ and $L(t)\sim t^{0.42}$. An estimation of the errors on these exponents is difficult due to correlations between data points. Mondello and Goldenfeld have previously simulated the 2D XY model with rather longer run times than we used [14]. Their data also provide evidence for different growth laws for different length scales for the time ranges they used.

TABLE II. Growth laws for the characteristic scale in O(n) systems. The values were obtained from the decay of the defect density.

Spatial dimension	2	2	3	3	3
Spin dimension	1	2	1	2	3
$1/z$	0.46	0.37	0.46	0.44	0.45

D. Short-distance results

1. The structure function tail amplitude

We now consider the predictions of Bray and Humayun for the amplitude of the power-law tail in the structure factor. We present only our results for vector systems, since a comparison to Ising simulations has already been made [10]. The scaling form for the structure factor is $S(k,t)=L^d(t)g(kL(t))$ and we expect a power-law tail of the form $[L(t)]^{-n}k^{-(d+n)}$. For large k, $S(k,t)k^{d+n}/\rho(t)$ should therefore be the constant predicted by Eq. (8). Using $L(t)=\rho^{-1/n}(t)$, the scaling variable is $k\rho^{-1/n}(t)$, which we plot against $S(k,t)k^{d+n}/\rho(t)=h(k\rho^{-1/n}(t))$, where $h(x)$ is a scaling

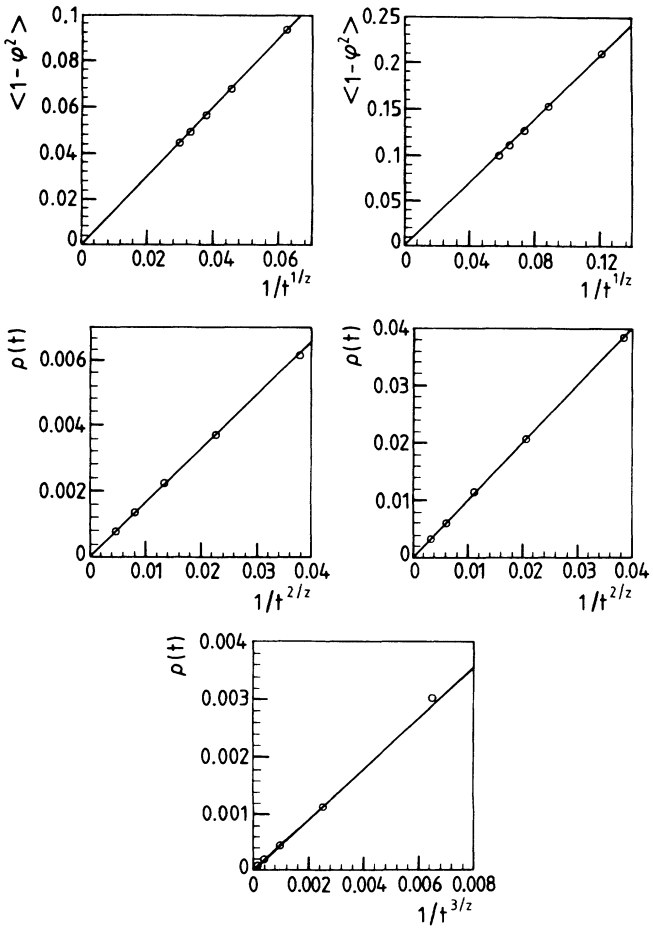

FIG. 7. Growth laws for the defect density in O(n) models. Moving left to right and top to bottom, (d,n) takes the values (2,1), (3,1), (2,2), (3,2), and (3.3).

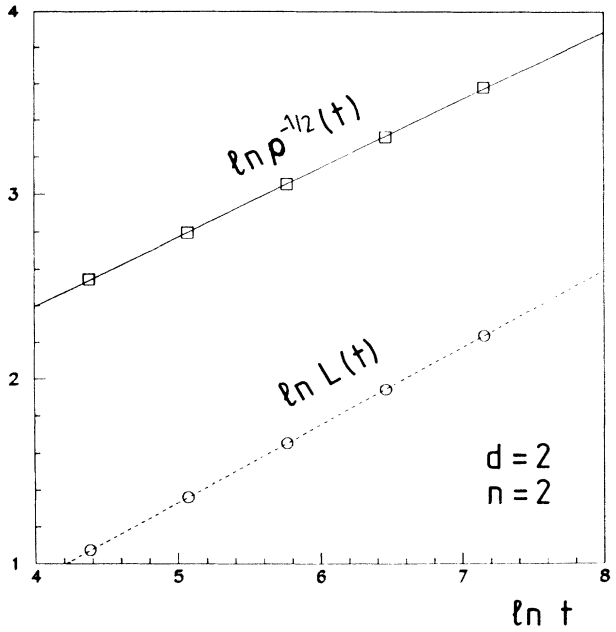

FIG. 8. Log-log plot of $[\rho(t)]^{-1/2}$ (top) and $L(t)$ (bottom) against time for the $d=2$ O(2) model. The straight lines have gradients 0.37 and 0.42 (top to bottom).

function. Figures 9 to 11 show these plots along with the analytic predictions for the large $k\rho^{-1/n}$ limit. Note that we have plotted $\langle S(k,t)k^{d+n}/\rho(t)\rangle$ rather than $\langle S(k,t)k^{d+n}\rangle/\langle\rho(t)\rangle$, because the calculated amplitude of the tail should be correct in each individual system. In all three cases, the numerical data are consistent with the predicted values of the tail amplitudes. For the largest values of k, there is a tendency of the data points to move up away from the predicted line. This is presumably because the calculations were carried out using a continuous order parameter field and at these large k, the effect

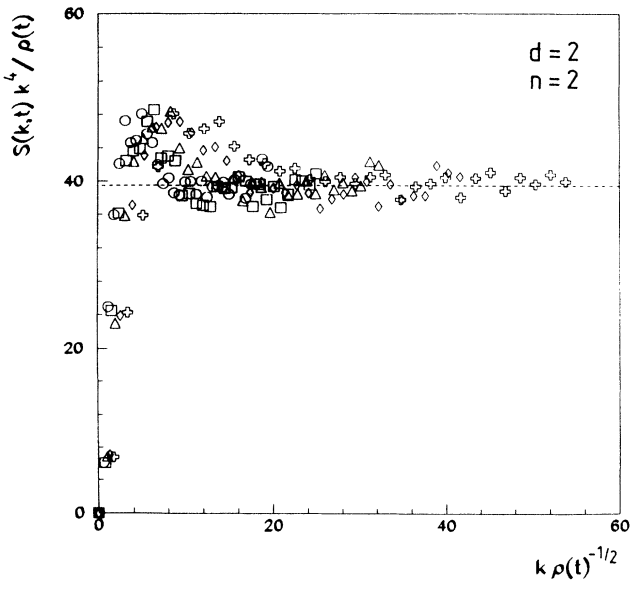

FIG. 9. Structure function of the $d=2$ O(2) model, with the power-law tail scaled out. The line is the exact result of Bray and Humayun for the amplitude of the tail.

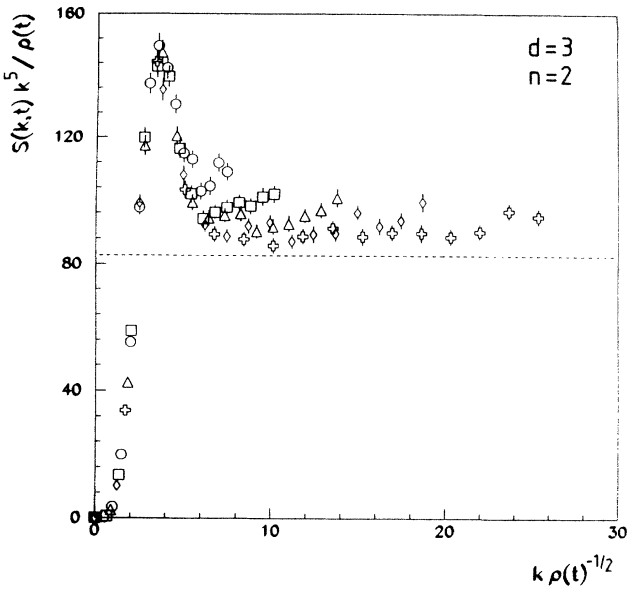

FIG. 10. Same as Fig. 9, but with $d=3$, $n=2$.

of the lattice becomes noticeable. The case $d=3$, $n=2$ shows a small but systematic discrepancy from the predicted values at large k. Again we attribute this to a lattice effect. In particular, the correction applied to the data to compare lengths measured on the lattice (Manhattan metric) to those calculated on the continuum (Euclidean metric) becomes inappropriate at length scales comparable to the lattice spacing. This effect accounts for the sign of the discrepancy in Fig. 10.

An interesting feature of the simulation curves is that they always approach their asymptotic constant value from above. For a scalar order parameter, Tomita [21] has accounted for this in terms of the curvature of the interfaces, but we are not aware of any similar calculations for vector fields. This same feature can also be seen when the data are plotted in the more usual form

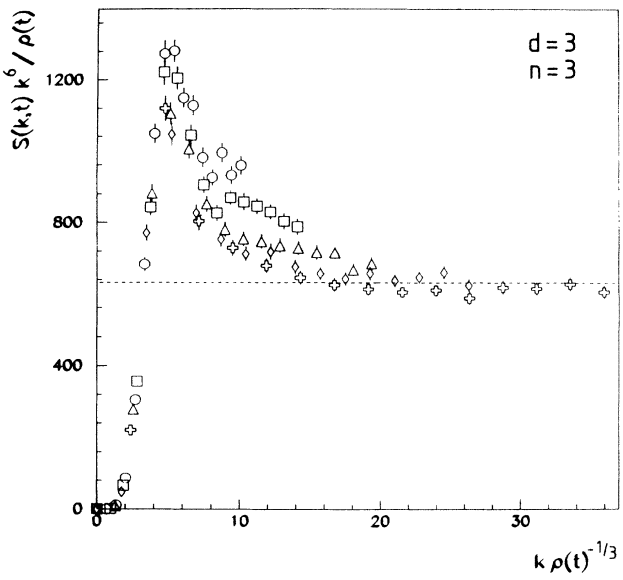

FIG. 11. Same as Fig. 9, but with $d=3$, $n=3$.

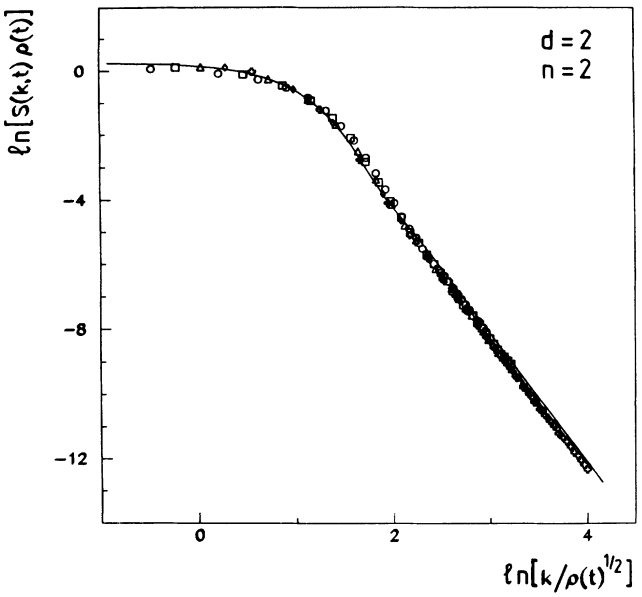

FIG. 12. Structure function of the $d=2$ O(2) model. The line is the curve calculated by BPT, scaled to give the best fit by eye.

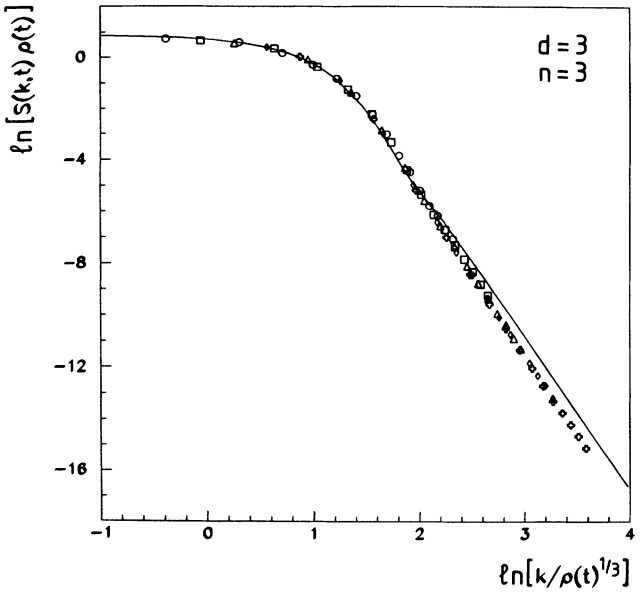

FIG. 14. Same as Fig. 12, but with $d=3$, $n=3$.

$\ln(L^{-d}(t)S(k,t))$ against $\ln(kL(t))$, although, because of the logarithmic scale, the effect is less pronounced. For completeness, we present the data replotted in this form in Figs. 12–14, along with the theoretical curve predicted by BPT. The rescaling factor introduced into the theoretical curves in these plots was the same as that used to give the best fit to the two-point correlation function in real space. Because this factor was determined using the whole of the two-point correlation function, the curves fit the data best at small k. Note that, since the data approach their asymptotic straight lines from above, there is a tendency in fitting data to assign too negative a slope to the structure factor tail.

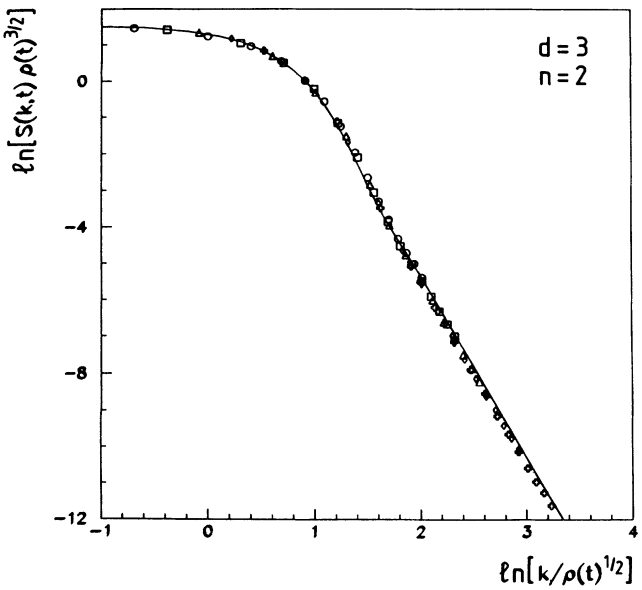

FIG. 13. Same as Fig. 12, but with $d=3$, $n=2$.

2. C_4 for the scalar systems

For $n=1$ and 2 we have exact predictions for the short-distance behavior of $C_4(r,t)$, the correlation function of the square of the order parameter. Plotting $C_4(r,t)$ against $C_2(r,t)$ gives a parameter-free scaling curve that can be used to test theories of phase ordering [16]. Here we will consider the short-distance behavior of these functions. From the previous section, we have for $n=1$,

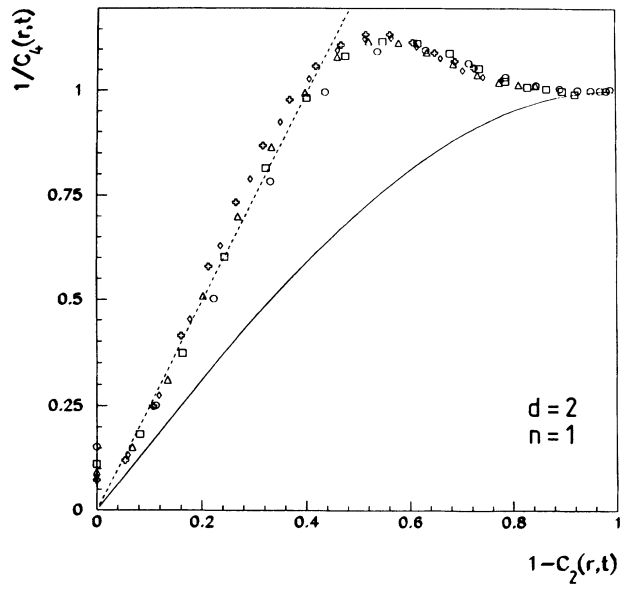

FIG. 15. Plot relating the correlation functions $C_2(r,t)$ and $C_4(r,t)$ for the 2D scalar model (data courtesy of S. Sattler). The straight line is the exact small r prediction and the curve is the OJK prediction [8,16].

$$C_2(r,t)=1-2\pi^{-1/2}\frac{\Gamma(d/2)}{\Gamma((d+1)/2)}\rho(t)r\ , \qquad a\ll r\ll L(t)\ , \quad (28)$$

$$C_4(r,t)=\frac{\Gamma(d/2)}{\pi^{1/2}\Gamma((d-1)/2)}\frac{1}{\rho(t)r},\quad a\ll r\ll L(t)\ ,$$

and so

$$C_4^{-1}(r,t)=\pi\frac{\Gamma((d-1)/2)\Gamma((d+1)/2)}{2\Gamma^2(d/2)}(1-C_2(r,t))\ , \quad (29)$$

in this regime. Therefore we expect a plot of $C_4^{-1}(r,t)$ against $1-C_2(r,t)$ to be linear near the origin with gradients $\pi^2/4$ and 2 for $d=2$ and $d=3$, respectively. Figures 15 and 16 show the data plotted in this manner for the 2D and 3D $n=1$ systems, along with a line of the appropriate gradient [22]. The data depart from the expected line for a very small r because we require $a\ll r\ll L(t)$. It does appear that for asymptotically large times the data will lie on the line we predict. It is also possible to calculate $C_4^{-1}(r,t)$ as a function of $1-C_2(r,t)$ using the approximate theories of Ohta, Jasnow, and Kawasaki (OJK) [4] and Mazenko [5] mentioned above. From Eq. (27) with $n=1$ one obtains $C_2(r,t)=(2/\pi)\sin^{-1}(\gamma)$ while [8,16] $C_4(r,t)=1/\sqrt{1-\gamma^2}$, where γ is the normalized two-point function for a Gaussian auxiliary field (see Refs. [8] and [16]). Eliminating γ gives the parameter-free relation

$$C_4^{-1}=\sin\left[\frac{\pi}{2}(1-C_2)\right]\ . \quad (30)$$

This prediction is included in Figs. 15 and 16. Plotting the data this way provides an absolute test of theory. Clearly, the existing theories based on a Gaussian auxiliary field are not quantitatively accurate. It is interesting to note, however, that for small r, i.e., small $1-C_2$, Eq. (30) gives the same linear relationship between C_4^{-1} and $1-C_2$ as the exact small r result in Eq. (29) does, and, moreover, the coefficients are the same in the limit $d\to\infty$. It is also clear from Figs. 15 and 16 that the data are closer to the predicted form in Eq. (30) for $d=3$ than for $d=2$. These facts add to the growing body of evidence that the OJK and Mazenko theories are exact in the large d limit [23]. Bray and Humayun [23] have recently discussed a procedure by which the leading order OJK result can in principle be systematically improved. The present data will provide a good test of any improvements to the theory.

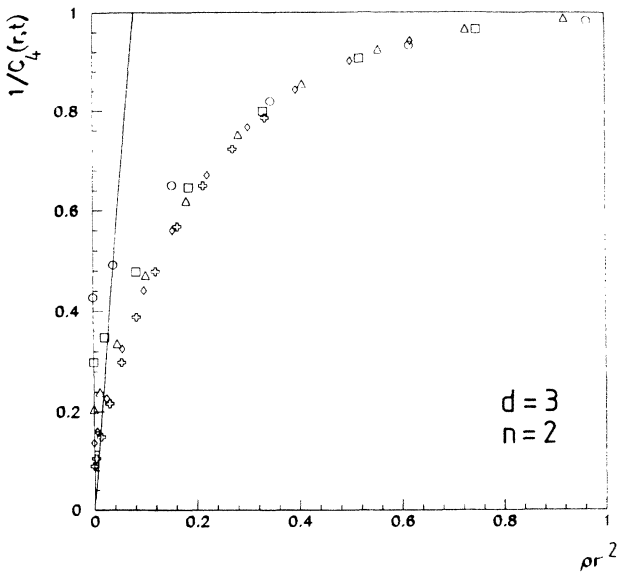

FIG. 17. The correlation function $C_4(r,t)$ for the 3D XY model. The straight line is the predicted small r behavior.

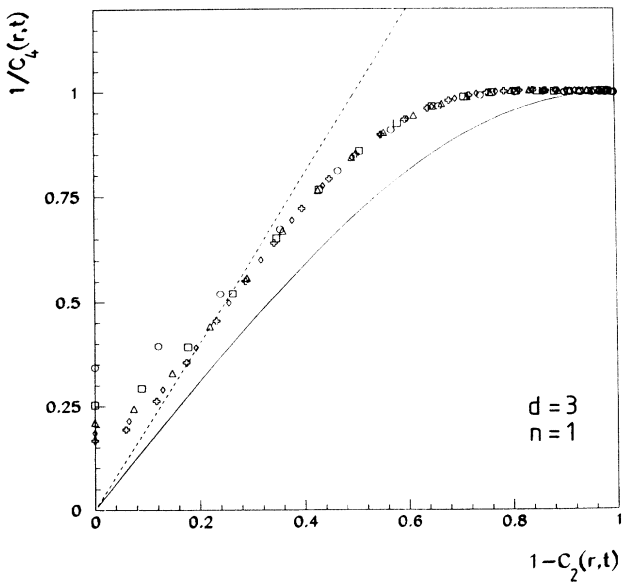

FIG. 16. Same as Fig. 15, but for the $d=3$ scalar model.

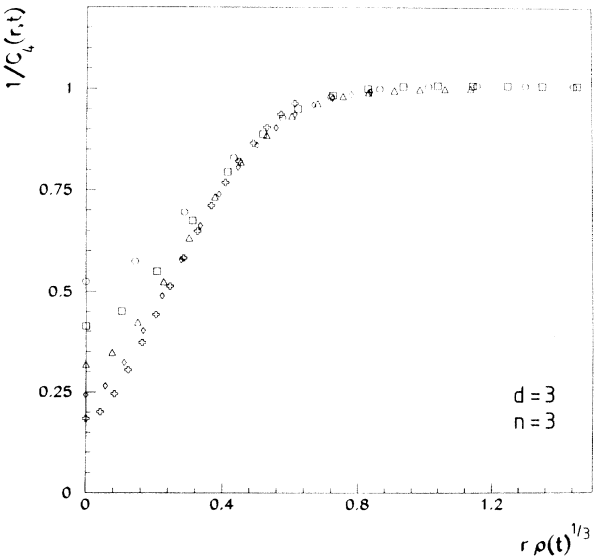

FIG. 18. The correlation function $C_4(r,t)$ for the $d=3$ O(3) model. The small r behavior is expected to be linear at asymptotically late times.

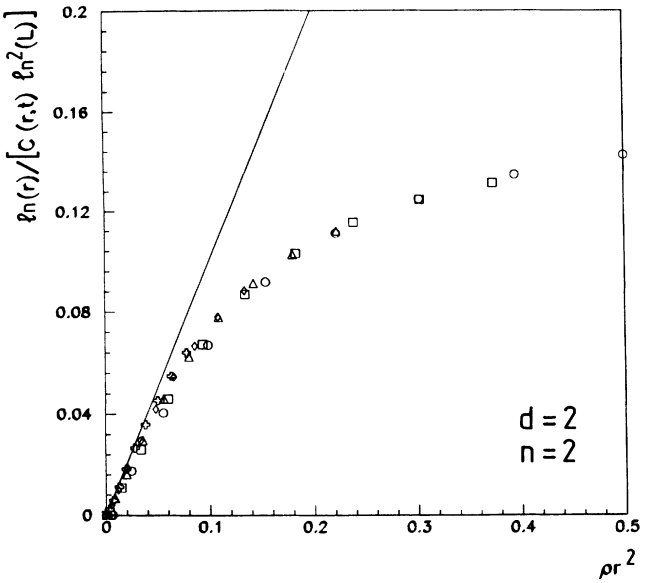

FIG. 19. The correlation function $C_4(r,t)$ for the 2D XY model. The straight line is the predicted small r behavior. We have used $L(t)=k\sqrt{\rho}$, where the parameter k was chosen to give the required gradient.

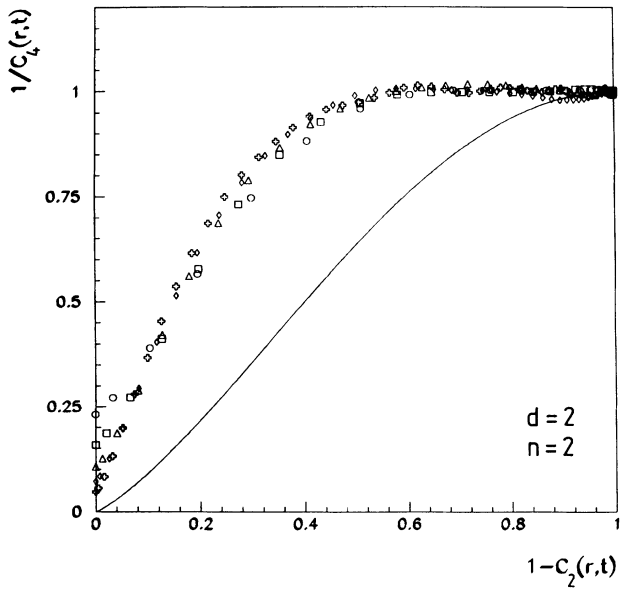

FIG. 21. Plot relating the correlation functions $C_2(r,t)$ and $C_4(r,t)$ for the 2D XY model. The curve is the BPT prediction [8,16].

3. C_4 for the XY model

From Sec. II we have, for $n=2$, the results given by Eqs. (23) and (24) for $C_4(r,t)$ for $d=2$ and $d>2$, respectively. Figure 17 shows the simulation data for $C_4(r,t)$ for the $d=3$ XY model plotted against the expected scaling variable ρr^2. The data scale well for large r and are consistent with the predicted short-distance behavior, $C_4^{-1}(r,t)=4\pi\rho r^2$.

We noted above that we cannot calculate $C_4(r,t)$ for the O(3) system because $\langle 1-\phi^2(r,t)\rangle$ is not determined by the field close to the defects. The result (20) for $C_4^N(r,t)=\langle[1-\phi^2(x,t)][1-\phi^2(x+r,t)]\rangle$ is still valid, however, although we cannot use it as an absolute prediction because the defect core size a is not known. From Eq. (20) we expect, for $n=3$, $C_4\sim 1/r$ for small r. The scaling function for $1/C_4$ should therefore be linear for small r, which is certainly consistent with the data shown in Fig. 18 (recalling that the data break away from the true scaling curve for small r, when the condition $r\gg a$ no longer holds).

For the $d=2$ XY model, we predicted in Sec. II that $C_4(r,t)$ would not scale for small r, but instead would

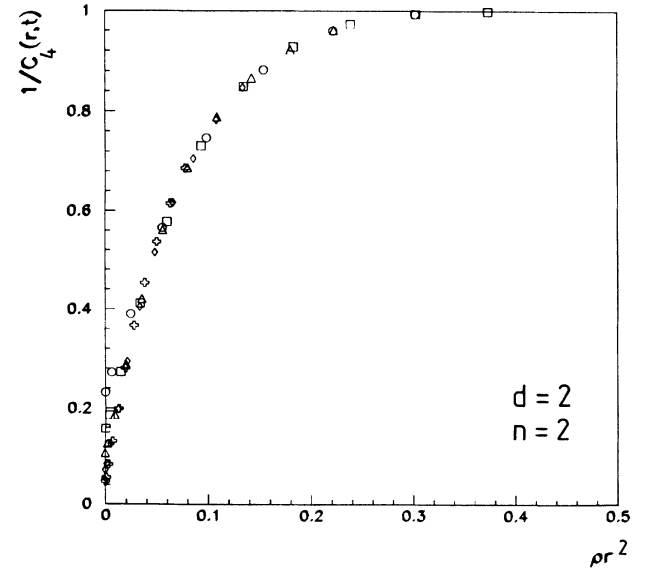

FIG. 20. The correlation function $C_4(r,t)$ for the 2D XY model plotted in the naive scaling form $1/C_4(r,t)$ against ρr^2.

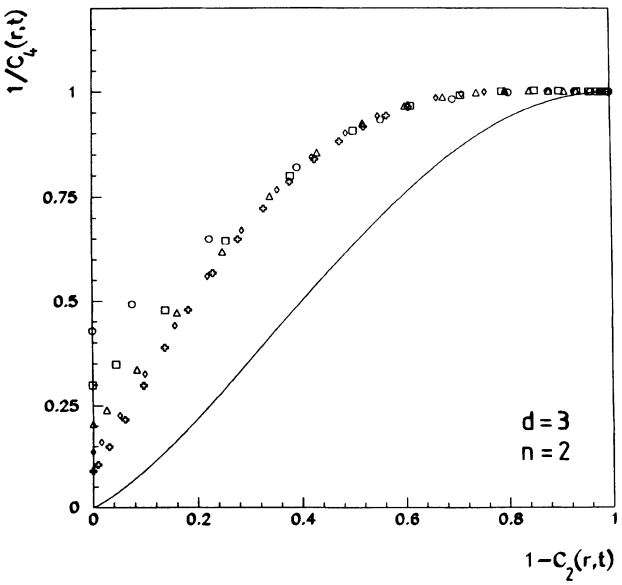

FIG. 22. Same as Fig. 21, but with $d=3$, $n=2$.

have the form given by Eq. (23). Figures 19 and 20 show the data plotted in the form predicted, and against the naive scaling variable ρr^2. In both cases the data appear to scale reasonably well. There is an ambiguity in the definition of $L(t)$, the characteristic scale, used in Fig. 19, so we have chosen $L(t)=1/\sqrt{2\rho}$, simply because this gives the best agreement with the prediction for the small r behavior. Different choices of $L(t)$ still give $C_4^{-1} \propto r^2$ for small r, but with different gradients. Our simulation results are therefore consistent with the predicted form of $C_4(r,t)$, although they do not constitute an absolute test. It is interesting that, in contrast to the two-point function, the data can be scaled using $\sqrt{\rho r^2}$. The deviations from scaling predicted by Eq. (23) are only logarithmic in $L(t)$, however, which does not vary greatly for the range of L available from the simulation. The fact that $C_4(r,t)$ can be approximately scaled using the defect density, whereas $C_2(r,t)$ cannot, may be because $C_4(r,t)$ is more closely associated with the defects. For $n=1$ systems, for instance, because the domain walls are sharp, C_4 is essentially a defect-defect correlation function.

Just as for the scalar systems, we can plot $1-C_2(r,t)$ against $1/C_4(r,t)$ to obtain a parameter-free test of the BPT result [2,3], Eq. (27), and the related theory of Refs. [7] and [6]. The equivalent result for C_4 was obtained in Ref. [8]: $C_4=F(1,1;n/2;\gamma^2)$. Eliminating γ between C_4 and C_2 gives C_4^{-1} as a function of $1-C_2$. Figures 21 to 23 show the data plotted in this form [22]. The data do not fit at all well quantitatively to the theoretical prediction, but do improve for larger d, as expected [23].

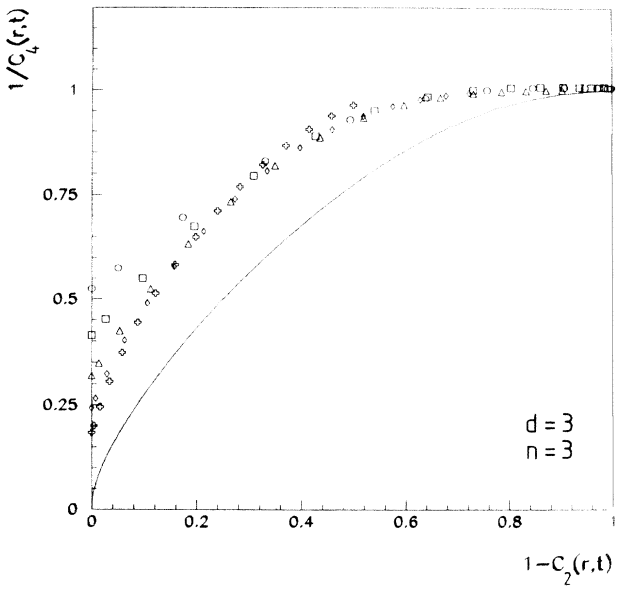

FIG. 23. Same as Fig. 21, but with $d=3$, $n=3$.

IV. CONCLUSIONS

We have performed numerical simulations of the O(n) model for $1 \le n \le d$ in dimensions $d=2$ and $d=3$. Exact calculations for the short-distance behavior of C_2 and C_4 have been compared to the simulation data and satisfactory agreement found. A particularly interesting feature of these exact results is that for the 2D XY model they predict a form for C_4 which cannot be expressed in a scaling form, a fact already noted by Bray in the context of his approximate calculation of C_4 [8]. Also, C_2 does not scale when plotted against $r\rho(t)^{1/2}$. We therefore suggest that there are logarithmic violations of scaling in this model.

ACKNOWLEDGMENTS

We thank S. Sattler for providing the data for the $n=1$ systems, and for discussions. R.E.B. thanks the SERC for financial support.

[1] The one-dimensional Glauber model can be solved exactly, and exhibits scaling: A. J. Bray, J. Phys. A **22**, L67 (1989); J. G. Amar and F. Family, Phys. Rev. A **41**, 3258 (1990). The nonconserved O(n) model can be solved for $n=\infty$ [see, e.g., G. F. Mazenko and M. Zannetti, Phys. Rev. B **32**, 4565 (1985)], and also scales.

[2] A. J. Bray and S. Puri, Phys. Rev. Lett. **67**, 2670 (1991).

[3] H. Toyoki, Phys. Rev. B **45**, 1965 (1992).

[4] T. Ohta, D. Jasnow, and K. Kawasaki, Phys. Rev. Lett. **49**, 1223 (1982).

[5] G. F. Mazenko, Phys. Rev. Lett. **63**, 1605 (1989); Phys. Rev. B **42**, 4487 (1990).

[6] A. J. Bray and K. Humayun, J. Phys. A **25**, 2191 (1992).

[7] Fong Liu and G. F. Mazenko, Phys. Rev. B **45**, 6989 (1992).

[8] A. J. Bray, Phys. Rev. E **47**, 228 (1993).

[9] For a general discussion of topological defects see L. Michel, Rev. Mod. Phys. **52**, 617 (1980); M. Kléman, *Points, Lines, and Walls, in Liquid Crystals, Magnetic Systems, and Various Ordered Media* (Wiley, New York, 1983).

[10] A. J. Bray and K. Humayun, Phys. Rev. E **47**, R9 (1993).

[11] G. Porod, in *Small-Angle X-ray Scattering*, edited by O. Glatter and O. Kratky (Academic, New York, 1982); P. Debye, H. R. Anderson, and H. Brumberger, J. Appl. Phys. **28**, 679 (1957); Y. Oono and S. Puri, Mod. Phys. Lett. B **2**, 861 (1988).

[12] This corresponds to a "positively charged" defect. For a "negatively charged" defect, obtained by globally inverting ($\phi_i \rightarrow -\phi_i$) an odd number of components of $\boldsymbol{\phi}$, the scalar product (4) is the same.

[13] A. Onuki, Phys. Rev. A **45**, 3384 (1992).

[14] M. Mondello and N. Goldenfeld, Phys. Rev. A **42**, 5865 (1990).

[15] A. J. Bray and A. D. Rutenberg, Phys. Rev. E **49**, 27 (1994).

[16] R. E. Blundell, A. J. Bray, and S. Sattler, Phys. Rev. E **48**, 2476 (1993).

[17] Y. Oono and S. Puri, Phys. Rev. A **38**, 434 (1988).

[18] I. M. Lifshitz, Zh. Eksp. Teor. Fiz. **42**, 1354 [Sov. Phys. JETP **15**, 939 (1962)]. S. M. Allen and J. W. Cahn, Acta Metall. **27**, 1085 (1979).

[19] A. J. Bray and K. Humayun, J. Phys. A **23**, 5987 (1990).

[20] M. Mondello and N. Goldenfeld, Phys. Rev. A **45**, 657

(1992); H. Toyoki, J. Phys. Soc. Jpn. **60**, 1153 (1991); **60**, 1433 (1991); H. Toyoki and K. Honda, Prog. Theor. Phys. **78**, 273 (1987); H. Toyoki, (unpublished).

[21] H. Tomita, Prog. Theor. Phys. **72**, 656 (1984).

[22] The same data were presented in a different way in [16]. The present method has the advantage that all the data appear on the plot, and the interesting short-distance region is concentrated near the origin.

[23] A. J. Bray and K. Humayun, Phys. Rev. E **48**, R1609 (1993).